Journal of Molecular Catalysis A: Chemical 404 (2015) 115–130

Contents lists available at ScienceDirect

Journal of Molecular Catalysis A: Chemical

journal homepage: www.elsevier.com/locate/molcata

Insight into the mechanism and possibility of ethanol formation from syngas on Cu(1 0 0) surface

Huayan Zheng, Riguang Zhang*, Zhong Li, Baojun Wang

Key Laboratory of Coal Science and Technology of Ministry of Education and Shanxi Province, Taiyuan University of Technology, Taiyuan 030024, Shanxi, PR China

ARTICLE INFO

Article history:
Received 9 April 2014
Received in revised form 22 January 2015
Accepted 20 April 2015
Available online 22 April 2015

Keywords:
Ethanol
Syngas
Mechanism
Cu(1 0 0)
Density functional theory

ABSTRACT

Low cost Cu-based catalysts have became an attractive option in catalyzing ethanol formation from syngas ($2CO + 4H_2 = C_2H_5OH + H_2O$). In this study, the complex mechanism of ethanol formation from syngas on Cu(1 0 0) surface has been investigated using density functional theory (DFT) calculations together with periodic slab models, in which all possible formation pathways of CH_x(x = 1–3) and C_2 oxygenates of ethanol precursor, as well as the hydrogenation of C_2 oxygenates to ethanol have been considered. Our results suggest that ethanol formation starts with CO hydrogenation to CHO, subsequently, CHO is further hydrogenated to CH_3O via CH_2O intermediate, CH_3O is eventually hydrogenated to CH_3OH; alternatively, CH_3O dissociation with hydrogen-assisted can also produce CH_3; then, CHO insertion into CH_3 can lead to the key intermediate CH_3CHO, which is successively hydrogenated to ethanol via CH_3CH_2O intermediates; moreover, among all reactions related to CH_3 species, CHO insertion into CH_3 to CH_3CHO is the most favorable reaction, which is responsible for C_2 oxygenates formation. In the overall process of ethanol synthesis, CH_3OH is more easily formed than CH_3, and ethanol formation is controlled by CH_3 formation, which means that the preferable CH_3OH formation rather than CH_3 is responsible for the low productivity and selectivity of ethanol. Therefore, aiming to obtain high productivity and selectivity to ethanol from syngas on Cu catalyst, we need to selectively modify Cu catalyst by using the promoters and/or supports, which should be able to boost CH_3 formation and/or suppress CH_3OH formation, this result can be applied to selectively modify and develop the novel Cu-based catalyst towards ethanol formation from syngas.

1. Introduction

Ethanol (C_2H_5OH) has been widely used as the feedstock for the synthesis of various products (e.g., chemicals, fuels, and polymers), meanwhile, it has also been commercially used as an additive and other applications [1–6]. Ethanol synthesis from syngas is one of the promising processes in industry [7–10]; however, a number of surface intermediates and competing elementary reactions is involved in this chemical process, the use of known catalysts still exhibits low yield and poor selectivity [7,11]. Thus, for ethanol synthesis from syngas, developing a efficient and high selective catalysts has become the focus of attention in this field.

Nowadays, Rh-based catalysts are the most studied systems and the only group of materials for syngas conversion into ethanol, rather than via methanol [12,13], in which two key steps is involved in ethanol formation, one is surface hydrocarbon CH_x(x = 1–3) formed by the direct CO dissociation or CO dissociation with hydrogen-assisted, the other is the C—C chain formation [7,11,14,15]. However, the expensive cost and limited supply of Rh-based catalysts have restricted their applications to be used as industrial catalysts [2,4]. Therefore, low cost Cu-based catalysts have became an attractive option, up to now, Cu-based catalysts have been widely used and produced good results for ethanol formation from syngas in the temperature range of 280–310 °C at pressures of about 40–100 bar [6,8,16–20].

As mentioned above, many experimental studies have been carried out to investigate ethanol formation from syngas on Cu-based catalysts; however, few studies at the molecular level for the formation mechanism of ethanol from syngas on Cu-based catalysts have been reported due to the complexity of the reactions. Recently, theoretical calculations have been widely used as a valuable tool to

* Corresponding author at: No. 79 Yingze West Street, Taiyuan 030024, PR China. Tel.: +86 351 6018239; fax: +86 351 6041237.
E-mail addresses: zhangriguang@tyut.edu.cn, zhangriguang1981@163.com (R. Zhang).

http://dx.doi.org/10.1016/j.molcata.2015.04.015
1381-1169/

probe into the mechanism of several typical reactions [21–27]. By means of theoretical calculation at the molecular level, a detailed investigation of ethanol formation from syngas on Cu catalyst will not only help us better illustrate the underlying mechanisms, but also provide a clue for selective modification of Cu-based catalysts to improve catalytic performance towards ethanol. Nowadays, only our previous studies by using density functional theory (DFT) calculations have investigated the CH_x formation from syngas on Cu(1 1 1) [28], the formation mechanism of C_2 oxygenates form syngas on Cu(1 1 0) [29]. In addition, ethanol formation from syngas on the stepped Cu(2 1 1) surface has been examined [30], however, all possible formation pathways of CH_x(x = 1–3) on Cu(2 1 1) have not been considered. More importantly, Cu particles primarily expose the Cu(1 1 1) and Cu(1 0 0) facets under reducing conditions (such as ethanol and methanol synthesis from syngas) [31]. Therefore, it is necessary to investigate ethanol formation from syngas on Cu(1 1 1) and Cu(1 0 0) surfaces.

In this study, the formation mechanism of ethanol from syngas on Cu catalyst have been systematically investigated by density functional theory (DFT) together with the periodic slab models, Cu catalyst is modeled by using Cu(1 0 0) surface (the reasons for the choice of Cu(1 0 0) surface is given in the main text). The mechanism includes all possible formation pathways of CH_x(x = 1–3) species, C—C chain of ethanol precursor, as well as ethanol, aiming to identify the preference mechanism, determine the key reaction intermediates, illustrate the function of Cu in ethanol formation, and provide as a clue for the selective modification of Cu-based catalyst to achieve high productivity and selectivity to ethanol, which may be also applied to other metal or alloy surfaces.

2. Computational details

2.1. Surface model

For Cu catalyst, TEM experiments have shown that under reducing conditions, Cu particles primarily expose Cu(1 1 1) and Cu(1 0 0) facets [31]. Meanwhile, for the RWGS reaction [32], CO_2 dissociation on Cu(1 0 0) surface is more easier than that on Cu(1 1 1). Further, DFT calculations by Wang et al. [33] show that the catalytic activity for water follows the order of Cu(1 0 0) > Cu(1 1 1). Above studies suggest that Cu(1 0 0) surface with the more open surface and more coordinative unsaturated sites is more active than Cu(1 1 1) surface. Thus, Cu(1 0 0) surface is employed to model the Cu catalyst in this study; in addition, the most stable face-centercubic (1 1 1) surface of close-packed Cu metal, Cu(1 1 1), has been also employed to investigate the catalytic behavior of the key steps involved in ethanol formation, as shown in Supplementary material.

Cu(1 0 0) surface is obtained from the experimental fcc crystal structure with the lattice parameter of 3.62 Å [31]. A periodic $p(3 \times 3)$ unit cell comprising nine atoms in each layer is used, which corresponds to an adsorbate surface coverage of a 1/9 of a monolayer (ML). Cu(1 0 0) surface is modeled using a three-layer slab model with a 15 Å vacuum between any two successive slabs. During the optimization, the atoms in the upper two layers together with the adsorbates are allowed to relax, whereas, the bottom layer is fixed at their bulk positions. As shown in Fig. 1, Cu(1 0 0) – [3 × 3] surface morphology has three different adsorption sites: Top Bridge and Hollow.

To confirm the sufficiency of a three-layer $p(3 \times 3)$ unit cell model, as shown in Table 1, we investigate the adsorption of key adsorbed species (CH_3O, CH_3OH, CO, CH_3CO and CH_3CHO) at their most stable sites on four-layer, five-layer and six-layer $p(3 \times 3)$ models (top two layers with adsorbates are relaxed, and other layers are fixed), our results suggest that the adsorption energies for several species is different with the change of slab layer, however, the difference for the adsorption energy is acceptable, which does not affect the trend of adsorption energy for these adsorbed species. Meanwhile, the key elementary reactions of CH_3 and CH_3OH formations starting from CH_3O are also discussed on $p(3 \times 3)$ model with different slab layers, as shown in Table 2, we still obtain that the activation barrier of CH_3 and CH_3OH formations starting from CH_3O is slightly different with the change of slab layer, however, CH_3OH is still more easily formed than CH_3. Thus, the number of Cu slab layer cannot obviously affect our qualitative analysis in this study.

Table 1
The comparisons for the adsorption energies (kJ mol^{-1}) of key adsorbed species on Cu(1 0 0) surface with the different slab layers.

Adsorbed species	$p(3 \times 3)$			
	6 layer	5 layer	4 layer	3 layer
CH_3O	283.2	287.2	288.1	286.9
CH_3OH	31.7	30.5	36.3	37.2
CO	92.5	81. 9	85.4	102.3
CH_3CO	175.0	170.5	186.8	188.0
CH_3CHO	22.4	20.9	26.7	26.4

Table 2
The comparisons for activation barrier and reaction energies (kJ mol^{-1}) of CH_3 and CH_3OH formations starting from CH_3O on Cu(1 0 0) surface with different slab layers and different cell size.

Elementary reaction		$p(3 \times 3)$				$p(3 \times 4)$
		6 layer	5 layer	4 layer	3 layer	3 layer
$CH_3O + H \rightarrow CH_3 + OH$	E_a	151.8	157.9	156.8	154.5	165.4
	$\triangle H$	−14.7	−18.7	−23.3	−16.2	−14.6
$CH_3O + H \rightarrow CH_3OH$	E_a	66.9	70.3	71.2	85.4	76.9
	$\triangle H$	−13.8	−7.9	−4.8	−3.4	4.5

On the other hand, to probe into the effect of cell size on the calculated results, the adsorption of the largest system CH_3CO at the most stable bridge site is investigated on the three-layer $p(2 \times 2)$, $p(2 \times 3)$, $p(3 \times 4)$ and $p(4 \times 4)$ models, respectively, which have the adsorption energies of 169.0, 170.4, 179.2 and 185.6 kJ mol^{-1}, respectively, these results suggests that the adsorption energy on $p(3 \times 4)$ (179.2 kJ mol^{-1}) and $p(4 \times 4)$ (185.6 kJ mol^{-1}) models are close to that (188.0 kJ mol^{-1}) on a $p(3 \times 3)$ model. Meanwhile, starting from CH_3O, the activation barrier and reaction energy of CH_3 and CH_3OH formations on the three-layer $p(3 \times 3)$ and $p(3 \times 4)$ model are calculated, suggesting that CH_3OH is more easily formed than CH_3, namely, the cell size of Cu slab layer can not obviously affect the qualitative comparison for the main reaction pathway.

Therefore, taking the calculation efficiency into consideration on Cu catalyst, in order to qualitatively understand the formation mechanism of ethanol from syngas, our calculated systems with a 3-layer $p(3 \times 3)$ model is suitable and enough, moreover, this model has been widely employed in the previous studies about the molecule adsorption and reaction mechanism on transition metal surfaces [34,35].

2.2. Calculation methods

Self-consistent periodic DFT calculations are performed using the Vienna ab initio simulation package (VASP) [36,37]. The interaction between ionic cores and electrons is described by the projector-augmented wave (PAW) method [38]. The exchange-correlation energy is calculated within the generalized gradient approximation (GGA) [39] together with the Perdew–Wang functional (GGA-PW91) [40]. A plane wave basis set is 400 eV to solve the Kohn–Sham equations. The Brillouin zone is sampled using

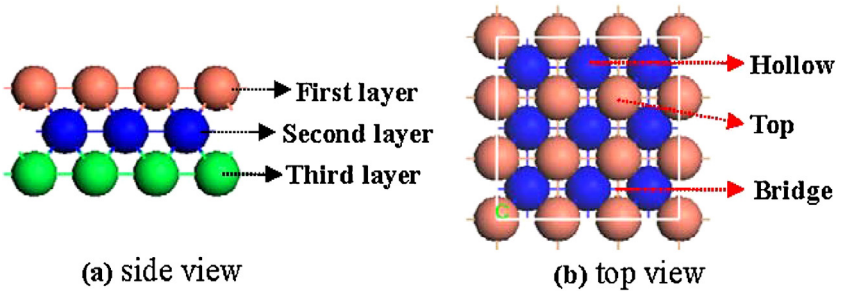

Fig. 1. The structure and adsorption sites of Cu(1 0 0) surface.

a $3 \times 3 \times 1$ Monkhorst–Pack *k*-point grid (11 *k*-points) [41] with Methfessel–Paxton smearing of 0.1 eV [42]. The relaxation of the electronic degrees of freedom is assumed to be converged, if the total energy change and the band structure energy change between two steps are both smaller than 10^{-5} eV. A forces difference between two steps less than 0.03 eV/Å is used as the criterion for convergence of ionic relaxation.

The climbing-image nudged elastic band method (CI-NEB) [43,44] is used to investigated the reactions paths. Transition states have been optimized using the dimer method [45,46]. The transition state is thought to be converged when the forces acting on the atoms are all small than 0.05 eV/Å for the various degrees of freedom set. In addition, in the discussion of the DFT results, no zero point energy (ZPE) corrections are included in this study. The molecules in the gas phase are calculated using a $10 \times 10 \times 10$ Å cubic unit cell.

On the other hand, to validate the reliability of the selected method, the geometrical parameters of CO molecule in gas phase are calculated using the different functionals (PW91, PBE and LDA), our results show that the length and stretching frequency of C—O bond using LDA functional are r_{C-O} = 1.135 Å and υ_{C-O} = 2180 cm^{-1}, respectively; those using PBE functional are r_{C-O} = 1.144 Å and υ_{C-O} = 2113 cm^{-1}, respectively; however, those values using PW91 functional are r_{C-O} = 1.142 Å and υ_{C-O} = 2125 cm^{-1}, respectively, which accords with the experimental values of 1.128 Å [47] and υ_{C-O} = 2138 cm^{-1} [48], and 2143 cm^{-1} [49–51], respectively, as well as other DFT calculated values 2121 cm^{-1} [48], and 2120 cm^{-1} [50]. As a result, GGA-PW91 functional is used throughout the present work.

3. Results and discussion

It is well known that syngas mainly contains CO and H_2 along with a small amount of CO_2 [52], meanwhile, the extensive studies about C_2H_5OH formation form syngas on Rh-based catalysts have been reported [7,9,11,15], in which only CO hydrogenation to form C_2H_5OH are considered. On the other hand, when CO_2 hydrogenation is considered to form C_2H_5OH, on the basis of the number of O atom in C_2H_5OH, we think CO_2 firstly needs to be converted to CO, then, CO hydrogenates to product C_2H_5OH. More importantly, since Cu catalyst shows a good catalytic activity toward CO_2 conversion to CO via the RWGS reaction [53], we can conclude that CO formation from CO_2 on Cu catalysts is facile, and C_2H_5OH synthesis is controlled by other key steps involving in CO hydrogenation to C_2H_5OH. As a result, in this study for C_2H_5OH formation from syngas, on the basis of above analysis, we skip CO_2 hydrogenation on Cu catalyst for C_2H_5OH synthesis, and only focus on CO hydrogenation to C_2H_5OH.

In this section, the formation mechanism of $CH_x(x = 1–3)$ species is firstly investigated to obtain the most favored form of CH_x species according to the proposed reaction network of $CH_x(x = 1–3)$ species formed from syngas. Then, starting from the most favored CH_x species, the possible formation pathways of C_2 oxygenates are discussed to obtain the preference mechanism. Further, the preference mechanism for the hydrogenation of the most favored C_2 oxygenates to C_2H_5OH is identified. Finally, we generally discuss the formations of $CH_x(x = 1–3)$ species, C_2 oxygenates and C_2H_5OH, as well as other mentioned reactions in C_2H_5OH formation.

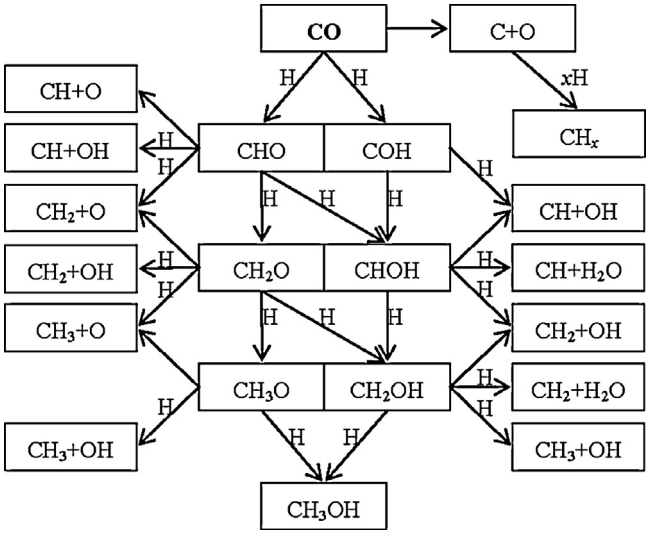

Fig. 2. The possible reaction network of $CH_x(x = 1–3)$ formation from syngas.

3.1. $CH_x(x = 1–3)$ formation from syngas

Previous studies have investigated CO hydrogenation and dissociation to C_1 oxygenates on different metal catalysts [23,27,31,54–57], as a result, the formation network of $CH_x(x = 1–3)$ from syngas on Cu(1 0 0) surface have been designed, which is similar with our previous studies on Cu(1 1 1) [28] and Cu(1 1 0) surface [29], as illustrated in Fig. 2, it includes all possible formation pathways of $CH_x(x = 1–3)$ species. In addition, we think that hydrogen atom is available for each hydrogenation step, and do not consider the energy needed to dissociate molecular hydrogen. By investigating the formation network of $CH_x(x = 1–3)$ species, an optimal formation path of $CH_x(x = 1–3)$ species can be obtained.

The most stable configurations of reactants and possible intermediates on Cu(1 0 0) surface are presented in Fig. 3, the corresponding energies and key geometric parameters are listed in Table 3. We can clearly obtain that the closed-shell species (such as CO, CH_3OH, CH_2O and H_2O) only weakly binds to Cu(1 0 0) surface, while other open-shell species strongly interact with the surface.

3.1.1. CO initial step

For CO initial step, as shown in Fig. 2, two possibilities exist: one is the formations of C and O by direct CO dissociation; the

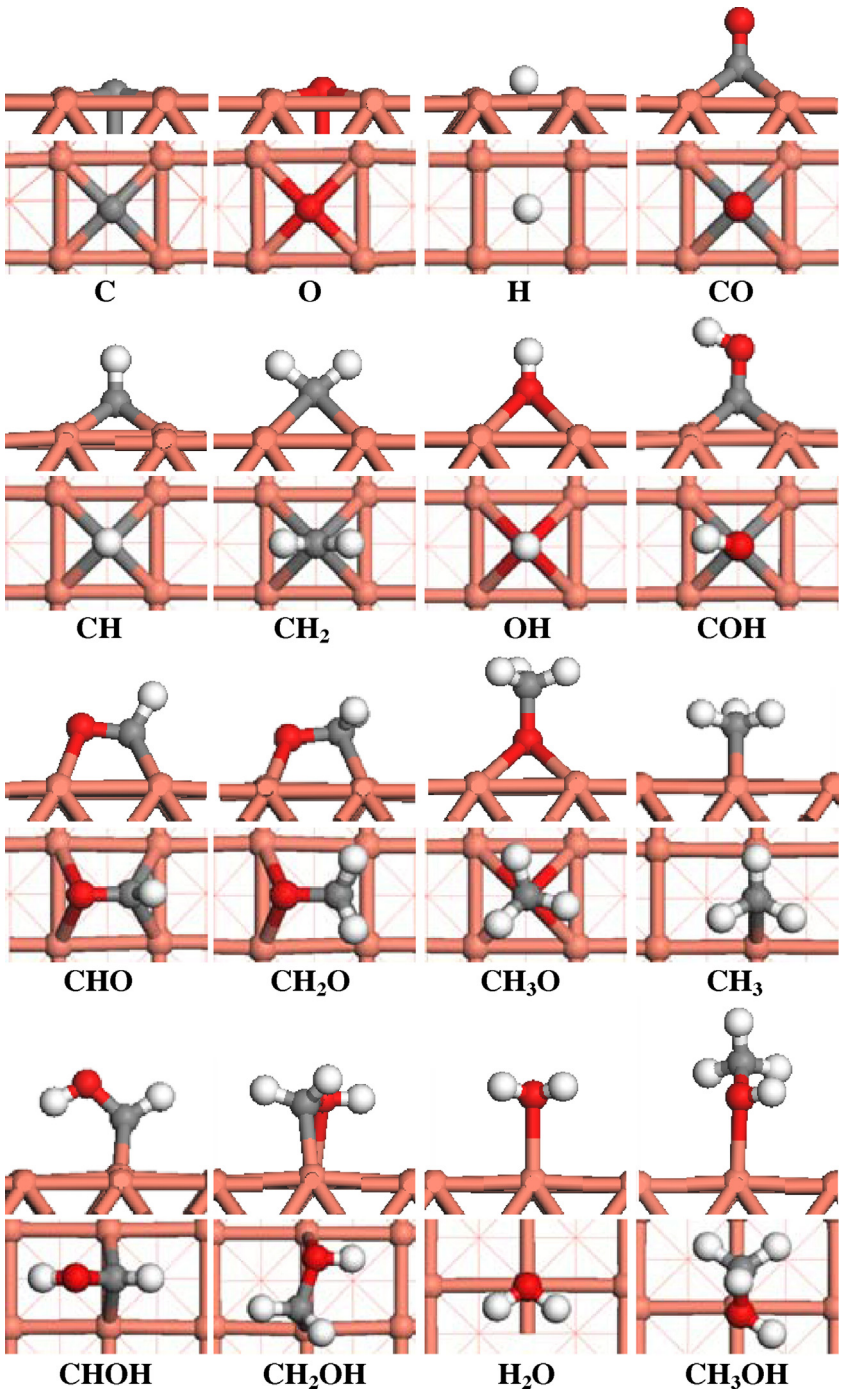

Fig. 3. The side and top views for the most stable adsorption configurations of reactants and all possible intermediates involved in the formation of CH_x(x = 1–3) species on Cu(1 0 0) surface. The C, O, H, and Cu atoms are shown in the grey, red, white, and orange balls, respectively. (For interpretation of the references to colour in this figure legend, the reader is referred to the web version of this article.)

other is the formations of COH or CHO by CO hydrogenation. Fig. 4 presents the potential energy diagram of these reactions together with the structures of initial states (ISs), transition states (TSs) and final states (FSs).

3.1.1.1. CO dissociation. In this step, the most stable adsorption configuration of CO is chosen as the initial state, which goes through the C—O bond scission via the transition state TS1 leading to final state, C + O; this reaction has a significantly high activation barrier of 391.1 kJ mol^{-1} with the high reaction energy of 112.4 kJ mol^{-1}, suggesting that the direct CO dissociation is very difficult to occur on Cu(1 0 0) surface.

3.1.1.2. CO hydrogenation. Starting from the initial state, CO + H, CO and H adsorb at the adjacent two hollow sites. For CHO formation, H adatom interacts with C atom of adsorbed CO via TS3. This reaction has an activation barrier of 100.9 kJ mol^{-1} with the reaction energy of 56.8 kJ mol^{-1}. For COH formation, an alternative CO hydrogenation via TS2, this reaction has a high activation barrier of 182.6 kJ mol^{-1} with the reaction energy of 70.8 kJ mol^{-1}.

Table 3
Adsorption energies and key geometric parameters for various species involved in CH_x(x = 1–3) formation on Cu(1 0 0) surface.

Species	E_{ads}/kJ mol^{-1}	Adsorption configuration	D_{Cu-X}/Å	Bonding details	
				Bond	Length/Å
C	736.0	Hollow: through C	1.91	—	—
O	672.5	Hollow: through O	2.00	—	—
H	360.6	Hollow: through H	1.88	—	—
CO	102.3	Hollow: through C	2.13	C—O	1.20
CH	600.5	Hollow: through C	1.99	C—H	1.11
CH_2	391.0	Hollow: through C	2.11	C—H	1.12
OH	377.5	Hollow: through O	2.17	O—H	0.98
COH	367.2	Hollow: through C	2.03/2.03/2.04/2.04	C—O/O—H	1.37/0.98
CHO	193.8	Hollow: C—B,O—B	2.03/2.04/2.14/2.15	C—O/C—H	1.31/1.11
CH_2O	54.8	Hollow: C—B,O—B	2.16/2.18/2.01/2.02	C=O/C—H	1.38/1.11
CH_3O	286.9	Hollow: through O	2.16/2.16/2.20/2.20	C—O/C—H	1.45/1.10
CH_3	214.4	Bridge: through C	2.08/2.19	C—H	1.11/1.10/1.10
CHOH	216.2	Bridge: through C	2.01/2.02	C—H/C—O/O—H	1.10/1.35/0.99
CH_2OH	169.6	Bridge: C-top O-top	2.00/2.21	C—H/C—O/O—H	1.09/1.46/0.98
H_2O	31.5	Top: through O	2.24	O—H	0.98
CH_3OH	37.2	Top: through O	2.11	C—H/C—O/O—H	1.10/1.45/0.98

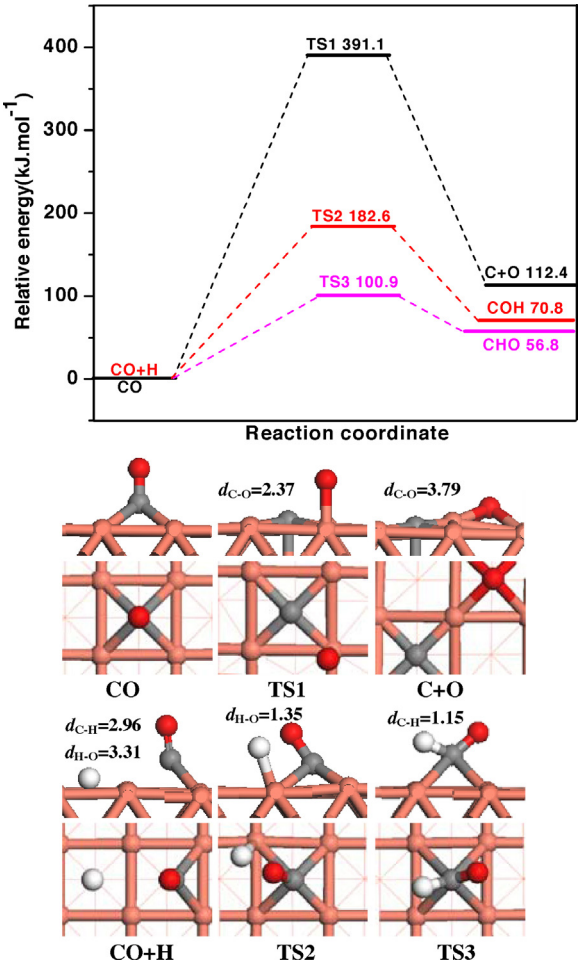

Fig. 4. The potential energy diagram of CO initial step together with the side and top views for the structures of initial states (ISs), transition states (TSs) and final states (FSs). Bond lengths are in Å. See Fig. 3 for color coding.

We can see from Fig. 4 that CHO is more easily formed both kinetically and thermodynamically than COH and CO dissociation, which means that CO hydrogenation on Cu(1 0 0) surface dominantly contributes to CHO formation. Thus, the formation of CH_x(x = 1–3) species is only considered starting from CHO species.

3.1.2. CH formation

Starting from CHO and CHO + H, as shown in Fig. 2, four pathways of CH formation exist: Path 1–1 is CHO dissociation into CH + O; Path 1–2 is CHO dissociation with hydrogen-assisted into CH + OH; Path 1–3 is CHO hydrogenation to CHOH, followed by its dissociation into CH + OH; Path 1–4 is CHO hydrogenation to CHOH, followed by its dissociation with hydrogen-assisted into CH + H_2O. Figs. 3 and 5 present the potential energy diagrams of these reactions together with the structures of ISs, TSs and FSs.

In Path 1–1, starting from CHO, and the C—O bond scission of CHO via TS1-1 leads to CH + O, both species bind at two adjacent hollow site; the distance between C and O atoms is increased from 1.31 Å in CHO to 1.89 Å in TS1-1 and 2.87 Å in CH + O; this reaction has a higher activation barrier of 134.3 kJ mol^{-1} with the reaction energy of 24.6 kJ mol^{-1}.

In Path 1–2, starting form CHO + H, the C—O bond scission of CHO with hydrogen-assisted can form CH + OH via TS1-2, the activation barrier of this reaction is 147.7 kJ mol^{-1}, it is exothermic by 56.5 kJ mol^{-1}.

In Path 1–3, starting from CHO + H, CHOH can be formed by H adatom interacting with the O atom of adsorbed CHO via TS1-3; the distances between H adatom and O decrease from 3.10 Å in CHO + H to 1.44 Å in TS1-3; this reaction has an activation barrier of 64.8 kJ mol^{-1} with the reaction energy of 32.0 kJ mol^{-1}; then, the C—O bond cleavage of CHOH form CH + OH via TS1-4. In TS1-4, CH and OH binds at the hollow and top sites, the distances between C and O atoms are 1.95 Å; this reaction is exothermic by 66.2 kJ mol^{-1} with an activation barrier of 88.5 kJ mol^{-1}.

In Path 1–4, similar to Path 1–3, CHO is firstly hydrogenated to CHOH, alternatively, the C—O bond scission of CHOH with hydrogen-assisted lead to CH + H_2O via TS1-5. In CH + H_2O, CH binds at the hollow site, H_2O plane is nearly parallel to Cu(1 0 0) surface, and is far away the surface; the distances between C and O atoms increase from 2.09 Å in TS1-5, 4.48 Å in CH + H_2O from 1.35 Å in CHOH + H, and the distances between H and O decrease from 3.44 Å in CHOH + H to 2.68 Å in TS1-5, 0.98 Å in CH + H_2O; this reaction has an activation barrier of 133.1 kJ mol^{-1} with the reaction energy of −65.2 kJ mol^{-1}. As shown in Fig. 5, we can obtain that Paths 1–1, 1–2, 1–3 and 1–4 have the highest barriers of 134.3, 147.7, 120.5 and 165.1 kJ mol^{-1}, and the reaction energies are 24.6, −56.5, −34.2 and −33.2 kJ mol^{-1}, respectively, these results show that Path 1–3 dominantly contributes to CH formation through the reaction process of CHO + H → CHOH → CH + OH, the corresponding rate-controlled step occurs at TS1-4, which has an activation barriers of 88.5 kJ mol^{-1}.

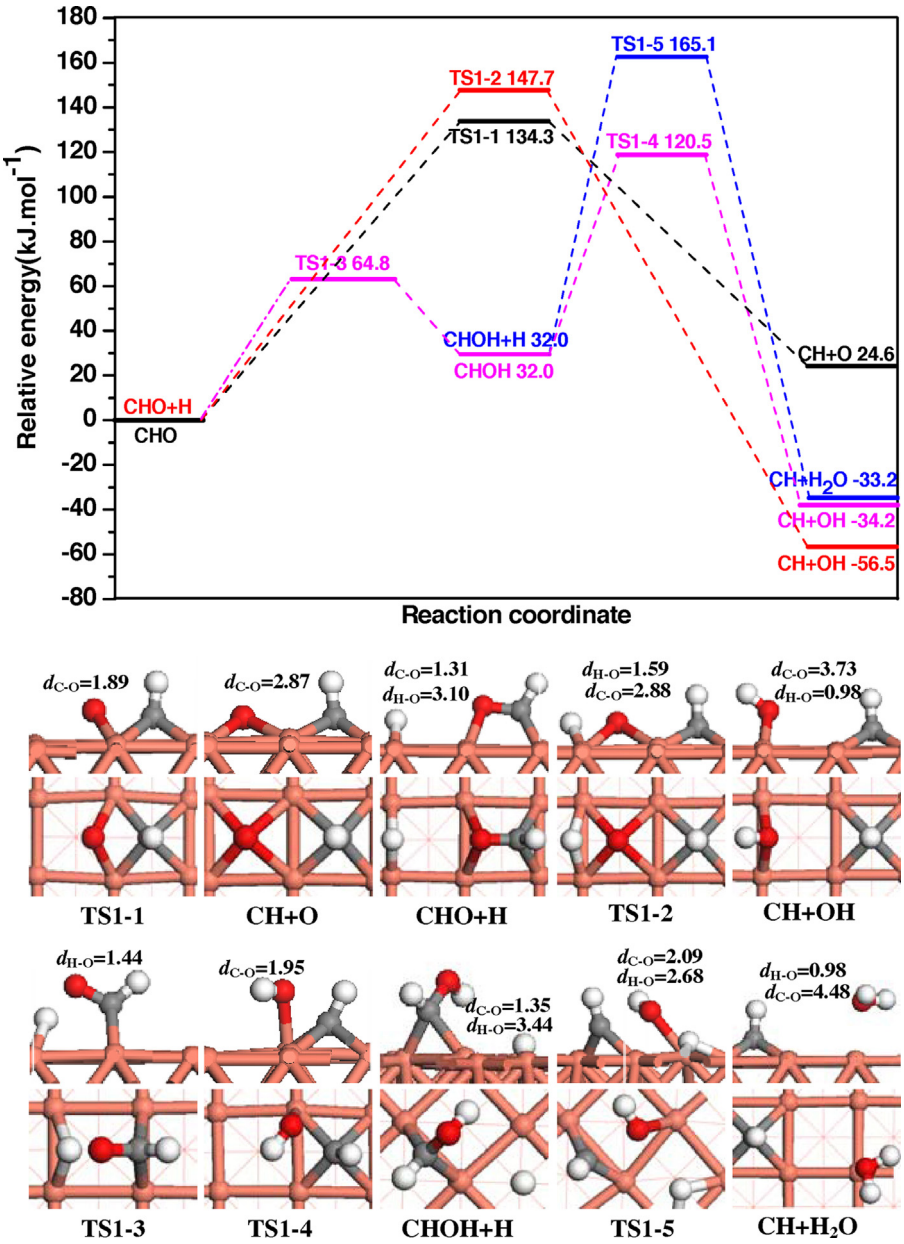

Fig. 5. The potential energy diagram of CH formation together with the side and top views for ISs, TSs and FSs. Bond lengths are in Å. See Fig. 3 for color coding.

3.1.3. CH_2 formation

For CH_2 formation, eight possible paths exist, as shown in Fig. 2; Figs. 3 and 6 present the potential energy diagram of these pathways together with the structures of ISs, TSs and FSs.

In Path 2–1, starting from CHO + H, the C—O bond scission of CHO with hydrogen-assisted can form CH_2 + O via TS2-1, which has an activation barrier of 118.9 kJ mol^{-1} with the reaction energy of 32.4 kJ mol^{-1}. In Path 2–2, CHO is first hydrogenated to CH_2O via TS2-2, the activation barrier and reaction energy are 49.6 and −39.7 kJ mol^{-1}, respectively; then, the C—O bond cleavage of CH_2O leads to CH_2 + O via TS2-3, which have the activation barrier and reaction energy of 186.5 and 72.1 kJ mol^{-1}, respectively. In Path 2–3, as described in Path 2–2, CHO is first hydrogenated to CH_2O; then, the C—O bond scission of CH_2O with hydrogen-assisted can form CH_2 + OH via TS2-4, this reaction has a high activation barrier of 170.7 kJ mol^{-1}, and it is exothermic by 19.8 kJ mol^{-1}.

In Path 2–4, similar to Path 1–3, CHO is first hydrogenated to CHOH; subsequently, the C—O bond scission of CHOH with hydrogen-assisted can form CH_2 + OH via TS2-5, the corresponding reaction energy is −71.8 kJ mol^{-1}, the activation barrier is 91.0 kJ mol^{-1}. In Path 2–5, similar to Path 1–3, CHO is firstly hydrogenated to CHOH; subsequently, CHOH hydrogenates to form CH_2OH via TS2-6 with the activation barrier and reaction energy of 38.0 and −48.6 kJ mol^{-1}, respectively; finally, the C—O bond cleavage of CH_2OH results in CH_2 + OH via TS2-8, this has an activation barrier of 108.8 kJ mol^{-1} with the reaction energy of −21.4 kJ mol^{-1}. For Path 2–6, similar to Path 2–2, CHO is firstly hydrogenated to CH_2O; subsequently, CH_2O hydrogenates to CH_2OH via TS2-7, which have the activation barrier and reaction energy of 95.5 and 3.4 kJ mol^{-1}, respectively; Further, the C—O bond scission of CH_2OH can form CH_2 + OH, as presented in Path 2–2. For Paths 2–7 and 2–8, similar to Paths 2–5 and 2–6, respectively, CHO is firstly hydrogenated to CH_2OH; then, the C—O bond cleavage of CH_2OH with hydrogen-assisted leads to CH_2 + H_2O via TS2-9, which has an activation barrier of 92.1 kJ mol^{-1}, and it is exothermic by 19.6 kJ mol^{-1}.

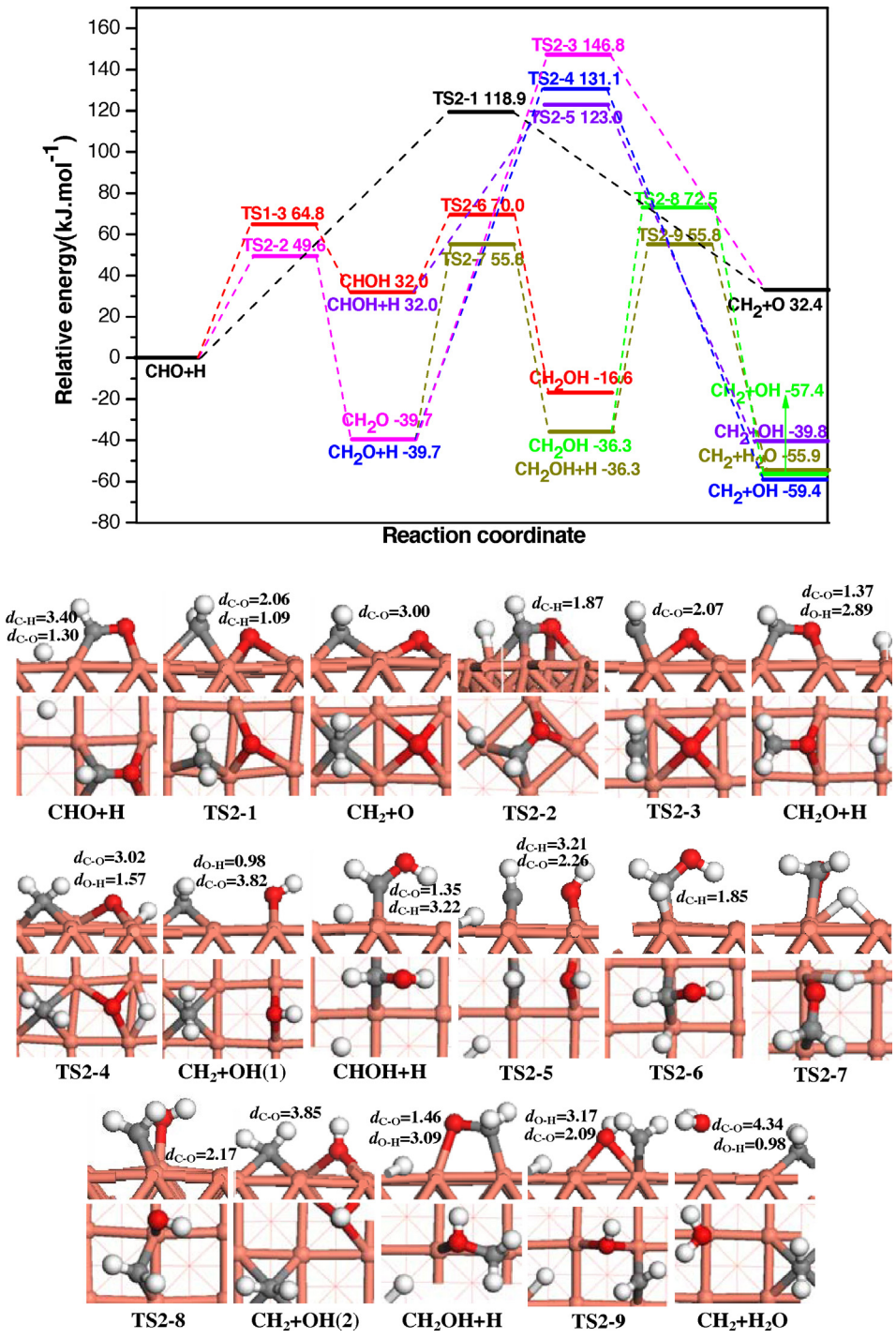

Fig. 6. The potential energy diagram of CH_2 formation together with the side and top views for ISs, TSs and FSs. Bond lengths are in Å. See Fig. 3 for color coding.

As shown in Fig. 6, we can obtain that the highest barrier (55.8 kJ mol^{-1}) of Path 2–8 is lower than those of other seven pathways, suggesting that Path 2–8 dominantly contribute to CH_2 formation by the reaction process of $CHO + 3H \rightarrow CH_2O + 2H \rightarrow CH_2OH + H \rightarrow CH_2 + H_2O$, the corresponding rate-controlled step occur at TS2-7 with an activation barrier of 95.5 kJ mol^{-1}.

3.1.4. CH_3 formation

For CH_3 formation, five possible paths exist, as shown in Fig. 2; Figs. 3 and 7 present the potential energy diagram of these pathways together with the structures of ISs, TSs and FSs.

In Path 3–1, similar to Path 2–2, CHO is first hydrogenated to CH_2O; subsequently, the C—O bond scission of CH_2O with hydrogen-assisted leads to $CH_3 + O$ via TS3-1, this reaction has an activation barrier of 152.8 kJ mol^{-1}, it is exothermic by 59.4 kJ mol^{-1}. In Path 3–2, similar to Path 2–2, CHO is first hydrogenated to CH_2O; subsequently, CH_2O is hydrogenated to CH_3O via TS3-2, the activation barrier and reaction energy are 28.4 and −77.4 k mol^{-1}, respectively; further, the C—O bond scission of CH_3O leads to $CH_3 + O$ via TS3-3, the activation barrier and reaction energy are 165.5 and 17.9 kJ mol^{-1}, respectively.

In Path 3–3, similar to Path 3–2, CHO is first hydrogenated to CH_3O; subsequently, the C—O bond scission of CH_3O with

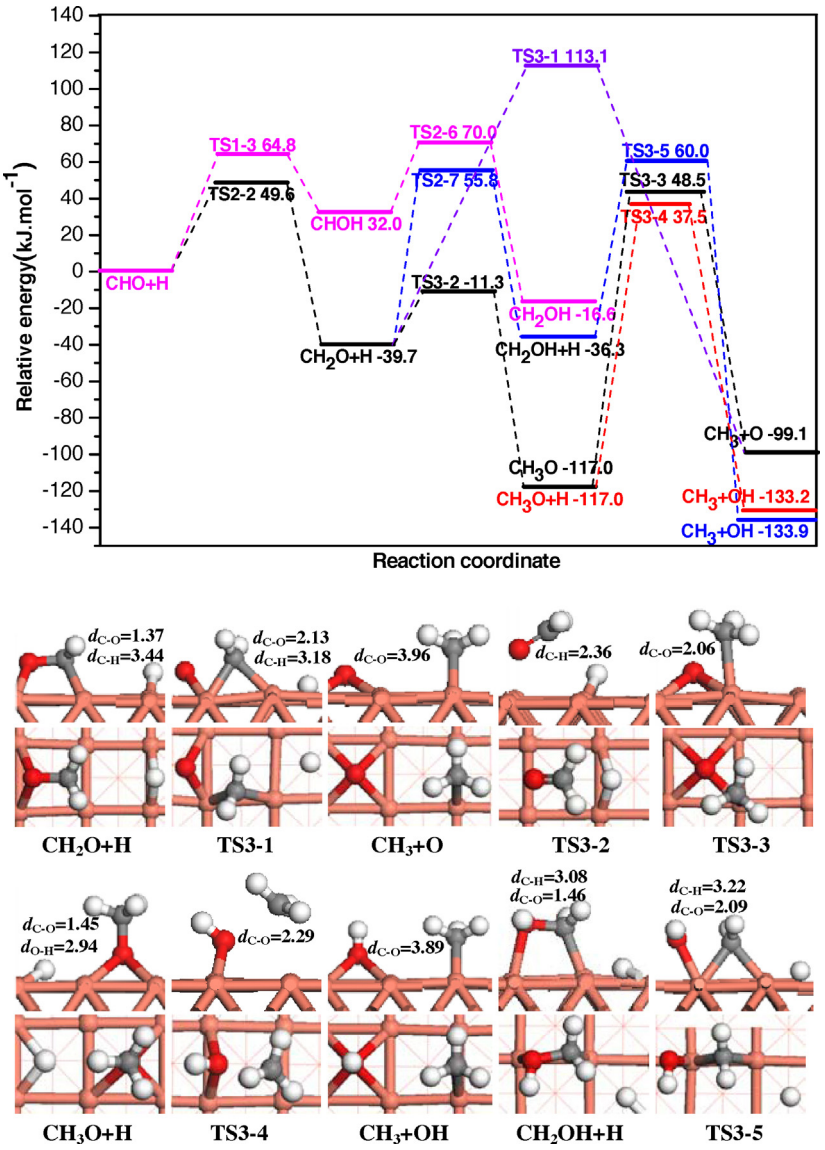

Fig. 7. The potential energy diagram of CH_3 formation together with the side and top views for ISs, TSs and FSs. Bond lengths are in Å. See Fig. 3 for color coding.

hydrogen-assisted lead to CH_3 + OH via TS3-4, this reaction has an activation barrier of 154.5 kJ mol^{-1}, it is exothermic by −16.2 kJ mol^{-1}. In Paths 3–4 and 3–5, as described in Paths 2–5 and 2–6, CHO is first hydrogenated via CHOH and CH_2O intermediates to CH_2OH; then, the C—O bond scission of CH_2OH with hydrogen-assisted results in CH_3 + OH via TS3-5, the activation barrier and reaction energy are 96.3 and −97.6 kJ mol^{-1}, respectively.

As shown in Fig. 7, we can obtain that the highest barriers (49.6 and 49.6 kJ mol^{-1}) of Paths 3–2 and 3–3 are lower than those of other pathways, however, the activation barrier (165.5 kJ mol^{-1}) of the rate-controlled step in Path 3–2 occurring at TS3-3 is larger than that for Path 3–3 (154.5 kJ mol^{-1}). Thus, Path 3–3 is dominantly responsible for CH_3 formation through the reaction process of CHO + 3H → CH_2O + 2H → CH_3O + H → CH_3 + OH.

3.1.5. Brief summary

On the basis of above results, we can obtain that CHO formation is more favorable both kinetically and thermodynamically than COH and CO dissociation for CO initial step. As a result, all CH_x(x = 1–3) species are formed starting with CHO or CHO + H on Cu(1 0 0) surface.

The potential energy diagram of the optimal paths of CH_x(x = 1–3) formation are illustrated in Fig. 8, with respect to CHO + H, we can see the highest barrier and reaction energy (49.6 and −133.2 kJ mol^{-1}) of CH_3 formation in a red line are lower than those of CH formation (120.5 and −34.2 kJ mol^{-1}) in a black line and CH_2 formation (55.8 and −55.9 kJ mol^{-1}) in a pink line, suggesting that CH_3 is much easily formed both kinetically and thermodynamically than CH and CH_2. Therefore, among all CH_x(x = 1–3) species, CH_3 is the most favorable monomer.

On the other hand, as mentioned above, CH_3O is formed by CH_2O hydrogenation, subsequently, the most favored monomer, CH_3, is formed by the reaction of CH_3O + H → CH_3 + OH, in which the hydroxyl OH will be also formed. Meanwhile, previous studies [58–60] have shown that on Cu and PdZn catalysts, OH can reacts very easily with CH_2O to form CH_2OOH, the reported activation energy barrier for this reaction on Cu(1 1 1) surface is 17 kJ mol^{-1} [58], or even 11 kJ mol^{-1} [59], as well as 15 kJ mol^{-1} on PdZn catalyst [60]. As a result, we further investigate the reaction of CH_2O + OH → CH_2OOH, our results show that this reaction has an activation barrier of 67.0 kJ mol^{-1}, and it is slightly endothermic by 1.9 kJ mol^{-1}. However, the reaction of CH_2O + H → CH_3O has a small activation barrier of 28.4 kJ mol^{-1}, and it is strongly exothermic

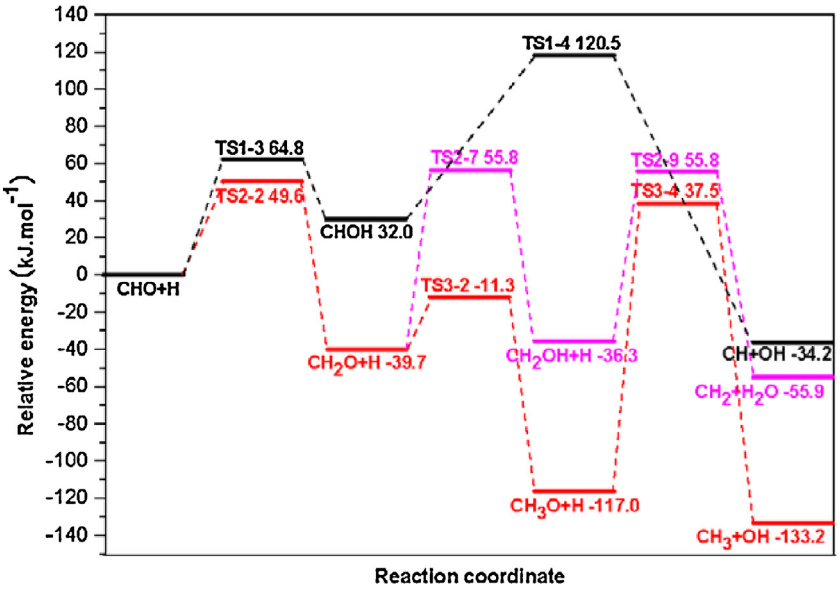

Fig. 8. The potential energy diagram for the optimal paths of CH_x(x = 1–3) formation starting from CHO hydrogenation.

by 77.4 kJ mol^{-1}. The activation barrier of $CH_2O + OH \rightarrow CH_2OOH$ is higher by 38.6 kJ mol^{-1} than that of $CH_2O + H \rightarrow CH_3O$, suggesting that CH_2O is more easily hydrogenated to CH_3O rather that being reacted with OH to CH_2OOH. In addition, we think that the OH involving in ethanol formation from syngas mainly reacts with H to form water.

3.2. CH_3OH formation and its effect on CH_3 formation

Above results suggest that all CH_x(x = 1–3) species come from the dissociation of CH_xO and CH_xOH intermediates formed by CHO hydrogenation, However, when above reactions occurs, since Cu catalyst can also exhibit good catalytic performance for CH_3OH formation from syngas [27], CH_xO and CH_xOH intermediates can also be hydrogenated to form CH_3OH As a result, CH_3OH formation by CHO hydrogenation is also investigated. Fig. 9 presents the potential energy diagram of CH_3OH formation together with the structures of ISs, TSs and FSs.

For Path 4–1, similar to Path 3–2, CHO is firstly hydrogenated to CH_3O via CH_2O intermediate; subsequently, CH_3O can be hydrogenated to CH_3OH via TS4-1, the activation barrier and reaction energy of this reaction are 85.4 and −3.4 kJ mol^{-1}. For Path 4–2, similar to Path 2–5, CHO is firstly hydrogenated to CH_2OH via CHOH intermediate; then, the hydrogenation of CH_2OH can form CH_3OH via TS4-2, this reaction has an activation barrier of 49.9 kJ mol^{-1}, it is exothermic by 85.2 kJ mol^{-1}. For Path 4–3, similar to Path 2–6, CHO is first hydrogenated to CH_2OH via CH_2O intermediate; then, CH_2OH hydrogenation can form CH_3OH via TS4-2.

As shown in Fig. 9 that the highest barrier (49.6 kJ mol^{-1}) of Path 4–1 in a red line is lower than those of other two pathways, meanwhile, the rate-controlled step of Path 4–1 occur at TS4-1, the activation barrier and reaction energy are 85.4 and −3.4 kJ mol^{-1}, respectively. Thus, Path 4–1 dominantly contributes to the formation of CH_3OH through the reaction process of $CHO + H \rightarrow CH_2O + H \rightarrow CH_3O + H \rightarrow CH_3OH$.

On the other hand, an optimal pathway for initial CO hydrogenation on Cu(1 0 0) surface is $CO + 3H \rightarrow CHO + 2H \rightarrow nCH_2O + H \rightarrow CH_3O$, which is also the common reaction pathway of CH_3 and CH_3OH formations. Fig. 10 summaries the potential energy diagram for the most favorable pathway of CH_3 and CH_3OH formation, it can be seen that the rate-controlled step of CH_3 formation occur at TS3-4 with the activation barrier of 154.5 kJ mol^{-1}, which is larger than that of CH_3OH formation (85.4 kJ mol^{-1}), suggesting that CH_3OH is more easily formed than CH_3. Since CH_x formation is thought to be a key step for C_2 oxygenates formation of C_2H_5OH precursor from syngas, more CH_x sources should be obtained for the formations of C_2H_5OH and hydrocarbons [3,7,29,61], namely, to achieve high productivity and selectivity to C_2H_5OH from syngas on Cu catalyst, more CH_3 should be boost and/or minimize CH_3OH formation.

3.3. C_2 oxygenates formation

For C_2 oxygenates formation, the studies on Rh and Co catalysts by Zhao et al. [15] found that CHO insertion into CH_x(x = 1–3) is superior and/or competitive to CO insertion and carbene coupling for chain growth; moreover, Choi and Liu [7] have found that CH_3 is the most favored monomer on Rh(1 1 1) surface among all CH_x(x = 1–3) species, meanwhile, the productivity and selectivity of C_2H_5OH is controlled by CH_3 hydrogenation to CH_4 formation and CO insertion into CH_3 to C_2 oxygenates. In this study, CH_3 are the most favored monomer formed by syngas on Cu(1 0 0) surface, in order to illustrate C_2 oxygenates formation, we further investigate CO insertion into CH_3, CHO insertion into CH_3, as well as CH_3 hydrogenation, dissociation and coupling on Cu(1 0 0) surface. Fig. 11 illustrates the potential energy diagram for these reactions together with the structures of ISs, TSs and FSs.

For CO insertion into CH_3, starting from CH_3 + CO, CH_3 and CO bind at the bridge and top sites, respectively; CO insertion into CH_3 can form CH_3CO via TS5-1. The distances of two C atom are decreased to 1.98 Å in TS5-1 from 3.66 Å in CH_3 + CO. This reaction has an activation barrier of 97.4 kJ mol^{-1}, it is exothermic by 19.9 kJ mol^{-1}. CH_3CO adsorbs at the bridge site via both C and O atoms with the adsorption energy of 188.0 kJ mol^{-1}.

For CHO insertion into CH_3, starting from CH_3 + CHO, CH_3 and CHO adsorb at the bridge and hollow sites, respectively; CHO insertion into CH_3 can form CH_3CHO via TS5-2. The distances of two C atom are decreased to 2.18 Å in TS5-2, from 3.89 Å in CH_3 + CHO. This reaction has an activation barrier of 41.9 kJ mol^{-1}, and it is largely exothermic by 96.4 kJ mol^{-1}. CH_3CHO locates at the top site via O atoms with only an adsorption energy of 26.4 kJ mol^{-1}.

For CH_3 hydrogenation, starting from CH_3+H, CH_3 and H bind at the bridge and hollow sites, respectively; CH_3 hydrogenation can

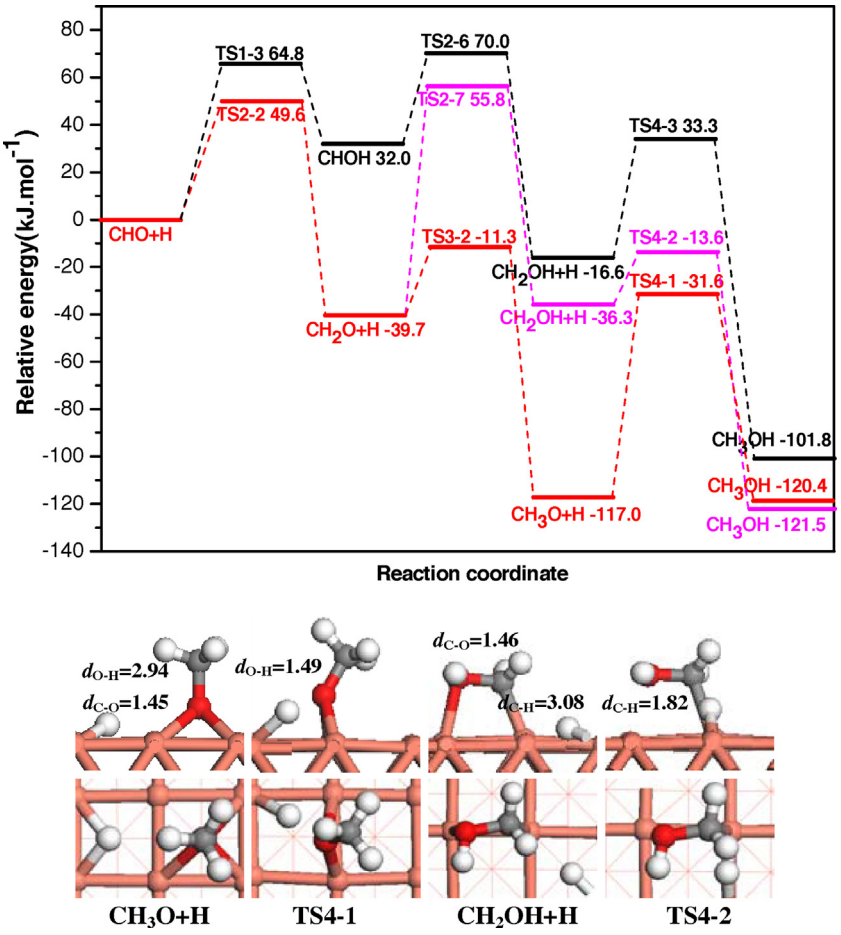

Fig. 9. The potential energy diagram for the optimal paths of CH_3OH formation by CHO hydrogenation together with ISs, TSs and FSs. Bond lengths are in Å. See Fig. 3 for color coding.

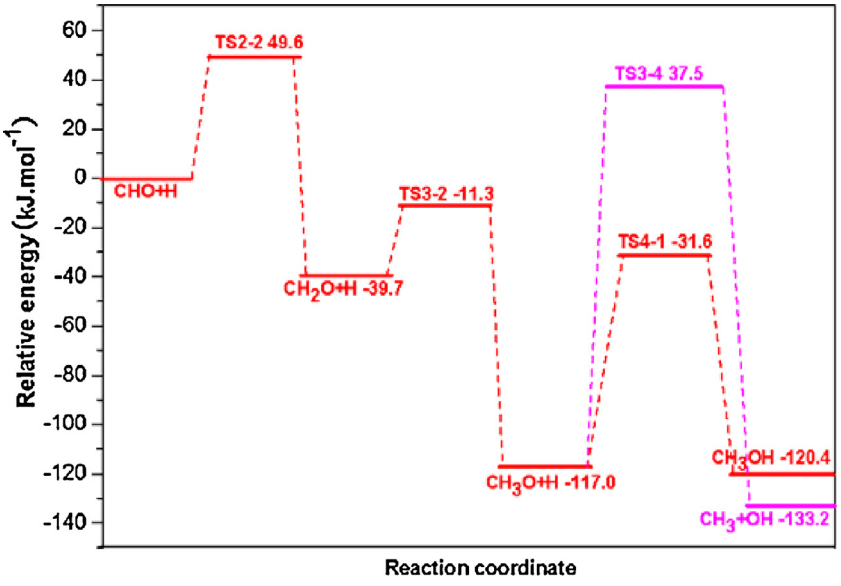

Fig. 10. The potential energy diagram for the most favorable paths of CH_3 and CH_3OH formations starting from CHO hydrogenation.

form CH_4 via TS5-3. The distance between C and H is decreased to 1.85 Å in TS5-3 from 3.25 Å in CH_3 + H. This reaction has an activation barrier of 77.9 kJ mol^{-1} with the large reaction energy of −71.1 kJ mol^{-1}. CH_4 is far away from the surface with only an adsorption energy of 6.4 kJ mol^{-1}.

For CH_3 dissociation CH_2 + H via TS5-4, this reaction has an activation barrier of 129.7 kJ mol^{-1}, and it is largely endothermic by 85.7 kJ mol^{-1}.

For CH_3 coupling, starting from CH_3 + CH_3, two CH_3 radical bind at the adjacent bridge site, CH_3 coupling can form C_2H_6 via

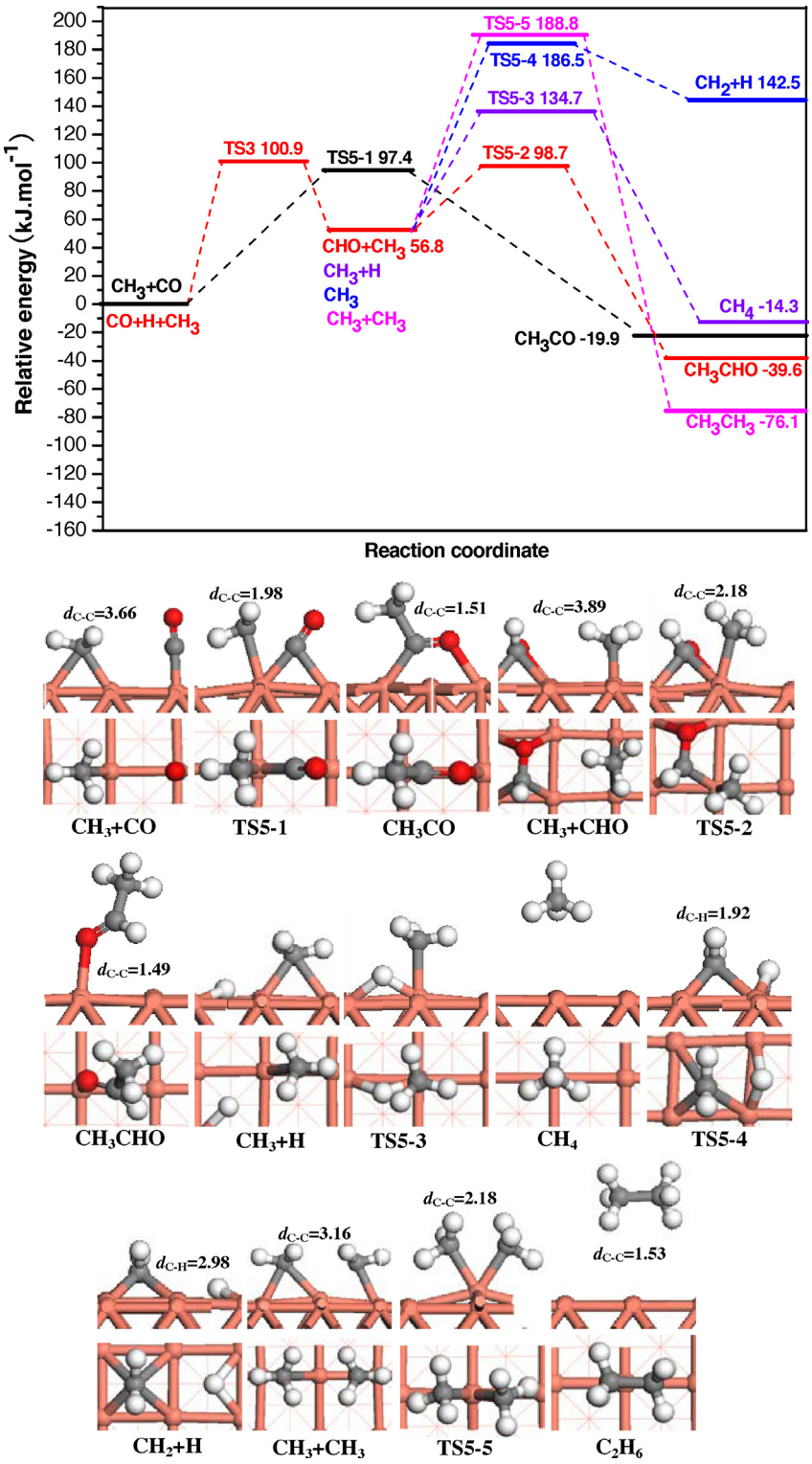

Fig. 11. The potential energy diagram of CO and CHO insertion into CH_3, as well as the hydrogenation, dissociation and coupling of CH_3 together with ISs, TSs and FSs on Cu(1 0 0) surface. Bond lengths are in Å. See Fig. 3 for color coding.

TS5-5. This reaction has an activation barrier of 132.0 kJ mol^{-1}, and it is largely exothermic by 132.9 kJ mol^{-1}. C_2H_6 is far away from the surface with only an adsorption energy of 19.1 kJ mol^{-1}.

Considering CHO formation by CO hydrogenation, as shown in Fig. 11, the highest barriers of CO insertion into CH_3, CHO insertion into CH_3, as well as CH_3 hydrogenation, dissociation and coupling are 97.4, 100.9, 134.7, 186.5 and 188.8 kJ mol^{-1}, respectively, which means that CO and CHO insertion into CH_3 to CH_3CO and CH_3CHO is two parallel and dominant reactions, which is dominantly responsible for C_2 oxygenates formation of ethanol precursor. More importantly, when CHO insertion into CH_3 to CH_3CHO (E_a = 41.9 kJ mol^{-1}, ΔH = −96.4 kJ mol^{-1}) occurs, CHO can also be hydrogenated to CH_2O, this reaction has an activation barrier of 49.6 kJ mol^{-1} with the reaction energy of −39.7 kJ mol^{-1},

suggesting that CHO hydrogenation to CH_2O is energetically compatible with CHO insertion into CH_3 to CH_3CHO, namely, partial CHO involves in hydrogenation to form CH_3 via the intermediates CH_2O and CH_3O, and the rest inserts into CH_3 to form CH_3CHO. Therefore, when more CH_3 is formed by CO hydrogenation, Cu(1 0 0) can exhibit a good catalytic activity and selectivity to C_2 oxygenates by CHO insertion into CH_3 rather than hydrocarbons.

In addition, the most stable face-center-cubic (1 1 1) surface of close-packed Cu metal, fcc(1 1 1), has been also employed to investigate the catalytic behavior of the key steps involved in ethanol formation. Fig. 12 presents the potential energy diagram of CO and CHO insertion into CH_3, as well as the hydrogenation, dissociation and coupling of CH_3 on Cu(1 1 1) surface, the detailed information on Cu(1 1 1) surface are given out in the Supplementary material. The calculated results show that the highest barriers of CO insertion into CH_3, CHO insertion into CH_3, as well as CH_3 hydrogenation, dissociation and coupling are 97.3, 131.9, 159.2, 201.3 and 247.8 kJ mol^{-1}, respectively, which means that CO insertion into CH_3 to CH_3CO is the dominant reactions for C_2 oxygenates formation; Secondly, CHO insertion into CH_3 to CH_3CHO is also responsible for C_2 oxygenates formation. Thirdly, the hydrocarbons are formed by the hydrogenation, dissociation and coupling of CH_3 species. Therefore, similar to Cu(1 0 0) surface, when more CH_3 is formed by CO hydrogenation, CH_3CO and CH_3CHO are the dominant existence form of C_2 oxygenates on Cu(1 1 1) surface.

3.4. C_2H_5OH formation

As mentioned above, CH_3CO and CH_3CHO are the dominant existence form of C_2 oxygenates. Thus, we continue to investigate the formation of C_2H_5OH by the successive hydrogenation of CH_3CO and CH_3CHO, respectively. Fig. 13 presents the potential energy diagram of CH_3CO and CH_3CHO hydrogenation to C_2H_5OH on Cu(1 0 0) surface together with the structures of ISs, TSs and FSs.

3.4.1. CH_3CO hydrogenation to C_2H_5OH

3.4.1.1. CH_3CO hydrogenation. One is CH_3CHO formation; the other is CH_3COH formation. Starting from $CH_3CO + H(1)$, CH_3CO can hydrogenate to CH_3CHO via TS6-1, this reaction has an activation barrier of 42.2 kJ mol^{-1}, and it is endothermic by 22.8 kJ mol^{-1}. Alternatively, beginning with $CH_3CO + H(2)$, CH_3CO can hydrogenate to CH_3COH via TS6-2, this reaction has an activation barrier of 74.1 kJ mol^{-1}, and it is endothermic by 41.7 kJ mol^{-1}. CH_3COH locates at the top site with an adsorption energy of 175.7 kJ mol^{-1}.

Above results show that CH_3CO hydrogenation to CH_3CHO is more easily formed both kinetically and thermodynamically than CH_3COH, suggesting that CH_3CHO is the dominant product of CH_3CO hydrogenation. So far, little information about key intermediates CH_3CO, CH_3CHO and CH_3COH in ethanol formation on Cu(1 0 0) surface is reported; only our previous studies shows that CH_3CO is the key intermediate for ethanol formation from syngas on Cu(2 1 1) surface [30], CH_2CO is the dominant form of C_2 oxygenates formed by syngas on Cu(1 1 0) surface [29]; these results show that the existence form of C_2 oxygenates on Cu-based catalyst is very sensitive to the structure of Cu surface.

3.4.1.2. CH_3CHO hydrogenation. One is to form CH_3CH_2O; the other is to form CH_3CHOH. Starting from $CH_3CHO + H(1)$, CH_3CH_2O is formed via TS6-3, which has an activation barrier of 29.3 kJ mol^{-1}, and it is exothermic by 60.1 kJ mol^{-1}; CH_3CH_2O locates at the hollow site an adsorption energy of 258.4 kJ mol^{-1}. Alternatively, starting from $CH_3CHO + H(2)$, CH_3CHOH can be formed via TS6-4, which has an activation barrier of 107.1 kJ mol^{-1}, and it is endothermic by 22.4 kJ mol^{-1}; CH_3CH_2O adsorbs at the hollow site with an adsorption energy of 258.4 kJ mol^{-1}.

Table 4
The activation barriers and reaction energies for the reactions of CO or CHO insertion into CH_3, CH_3 hydrogenation to CH_4, as well as CH_3 and CH_3OH formations on Cu and Rh surfaces.

Surface	Elementary reaction	E_a/kJ mol^{-1}	ΔH/kJ mol^{-1}
Cu(1 0 0)	$CH_3 + CHO \rightarrow CH_3CHO$	41.9	−96.4
	$CH_3 + H \rightarrow CH_4$	77.9	−71.1
	$CH_3O + H \rightarrow CH_3 + OH$	154.5	−16.2
	$CH_3O + H \rightarrow CH_3OH$	85.4	3.4
Rh(1 1 1)[a]	$CH_3 + CO \rightarrow CH_3CO$	89.7	14.5
	$CH_3 + H \rightarrow CH_4$	55.0	−19.3
	$CH_3O \rightarrow CH_3 + O$	102.3	−18.3
	$CH_3O + H \rightarrow CH_3OH$	88.8	3.9

[a] The studies by Choi and Liu in Ref. [7].

Above results show that for CH_3CHO hydrogenation, CH_3CH_2O is more easily formed both favorable both kinetically and thermodynamically compared to CH_3CHOH, namely, CH_3CH_2O is the dominant product for CH_3CHO hydrogenation on Cu(1 0 0) surface.

3.4.1.3. CH_3CH_2O hydrogenation to C_2H_5OH. For CH_3CH_2O hydrogenation, starting from $CH_3CH_2O + H$, CH_3CH_2O hydrogenation can form C_2H_5OH via TS6-5. This reaction has an activation barrier of 70.8 kJ mol^{-1}, and it is slightly endothermic by 6.0 kJ mol^{-1}. C_2H_5OH leaves away from the surface with only an adsorption energy of 24.1 kJ mol^{-1}.

3.4.2. CH_3CHO hydrogenation to C_2H_5OH

As described in CH_3CO hydrogenation to form C_2H_5OH, CH_3CHO hydrogenation prefers to form CH_3CH_2O, then, CH_3CH_2O hydrogenation leads to C_2H_5OH. Thus, the pathway for CH_3CHO hydrogenation to C_2H_5OH is that $CH_3CHO + 2H \rightarrow CH_3CH_2O + H \rightarrow C_2H_5OH$.

3.4.3. Comparisons of the key step for C_2H_5OH formation between Cu and Rh surfaces

Previous DFT studies by Choi and Liu [7] have investigated ethanol formation from syngas on Rh catalyst; aiming to understand the catalytic efficiency of Cu in ethanol formation, we further qualitatively compare the key reaction steps of ethanol formation between Cu catalyst with those reported results on Rh catalyst, Table 4 lists the corresponding activation barrier and reaction energy of key steps on Cu and Rh surfaces.

We can obtain that $CO + 3H \rightarrow CHO + 2H \rightarrow CH_2O + H \rightarrow CH_3O$ on Cu and Rh surfaces is the common optimal pathway, and CH_3OH is more easily formed than CH_3. Starting from CH_3, Choi and Liu have found that on Rh(1 1 1) surface, CH_4 is more easily formed than CH_3CO via CO insertion into CH_3. However, Cu(1 0 0) surface in this study show that CHO insertion into CH_3 to CH_3CHO is more favorable than CH_4 formation; meanwhile, our previous studies on Cu(2 1 1) surface also show that CH_3CO formed by CHO insertion into CH_3 is more favorable than CH_4 formation [30]; these results means that Cu catalyst can exhibit a better selectivity to C_2 oxygenate of C_2H_5OH precursor rather than CH_4, this is different from that on Rh catalyst.

3.5. General discussions

Fig. 14 presents the optimal reaction pathway of C_2H_5OH formation from syngas on Cu(1 0 0) surface. It can be seen that C_2H_5OH formation on Cu(1 0 0) surface is to first produce CH_3 species via the process of $CO + 4H \rightarrow CHO + 3H \rightarrow CH_2O + 2H \rightarrow CH_3O + H \rightarrow CH_3 + OH$, then, CHO insertion into CH_3 can form CH_3CHO, and followed by successive hydrogenation to C_2H_5OH. CH_3 formation via the reaction of $CH_3O + H \rightarrow CH_3 + OH$ is the rate-limiting step of the overall

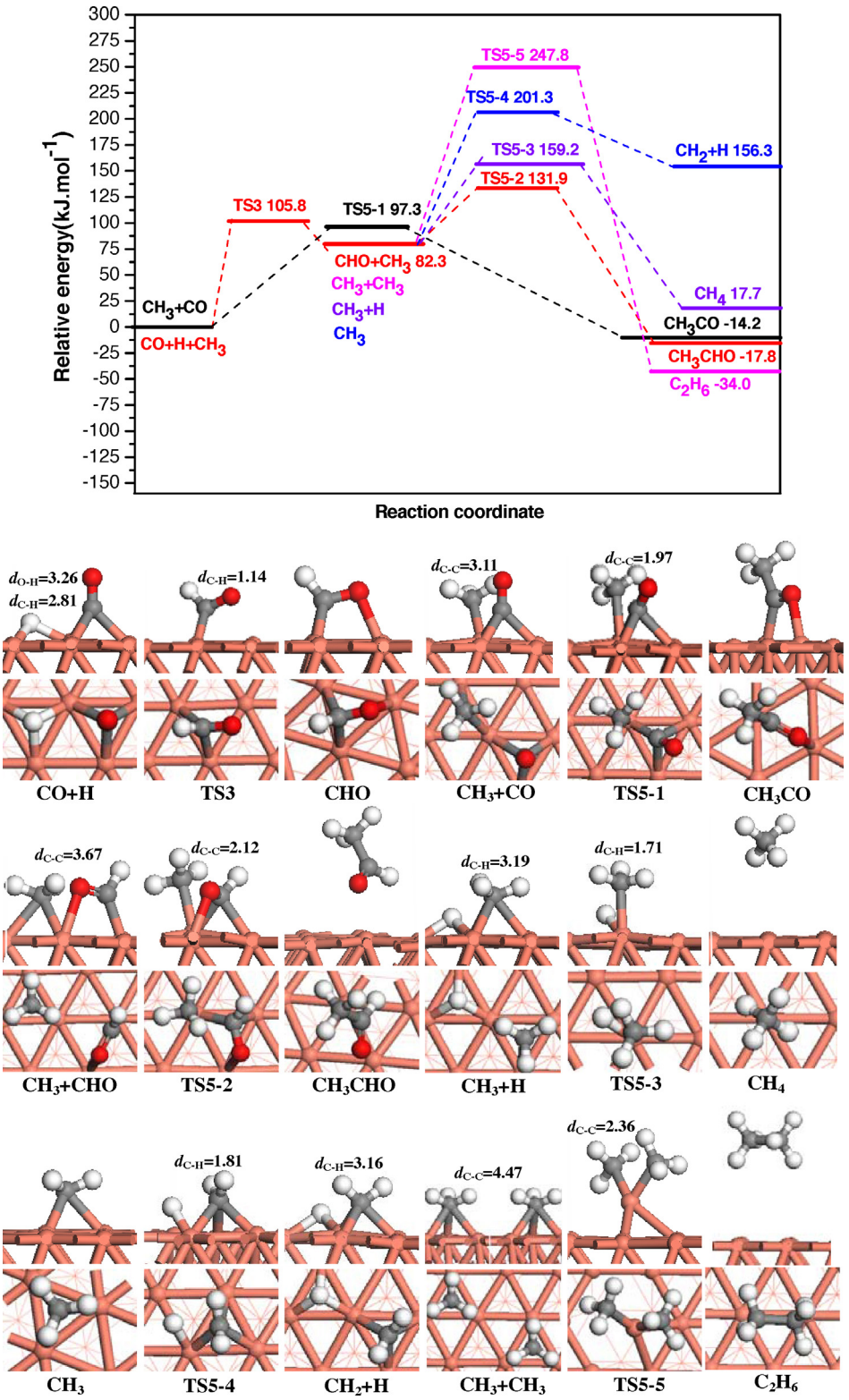

Fig. 12. The potential energy diagram of CO and CHO insertion into CH_3, as well as the hydrogenation, dissociation and coupling of CH_3 together with ISs, TSs and FSs on Cu(1 1 1) surface. Bond lengths are in Å. See Fig. 3 for color coding.

conversion with a significantly high activation barrier of 154.5 kJ mol^{-1}. Meanwhile, CH_3OH can be formed by the reaction process of $CO + 4H \rightarrow CHO + 3H \rightarrow CH_2O + 2H \rightarrow CH_3O + H \rightarrow CH_3OH$, and the reaction of $CO + H \rightarrow CHO$ is the rate-limiting step with an activation barrier of 100.9 kJ mol^{-1}. Further, compared to CHO insertion into CH_3 to CH_3CHO, the formations of CH_4, CH_2 and C_2H_6 by the hydrogenation, dissociation and coupling of CH_3 are all very difficult to occur due to the high activation barrier.

Our results on Cu(1 0 0) surface show that CH_3OH is the main product from syngas, which accords with the general fact that Cu catalyst can exhibit good catalytic performance for CH_3OH

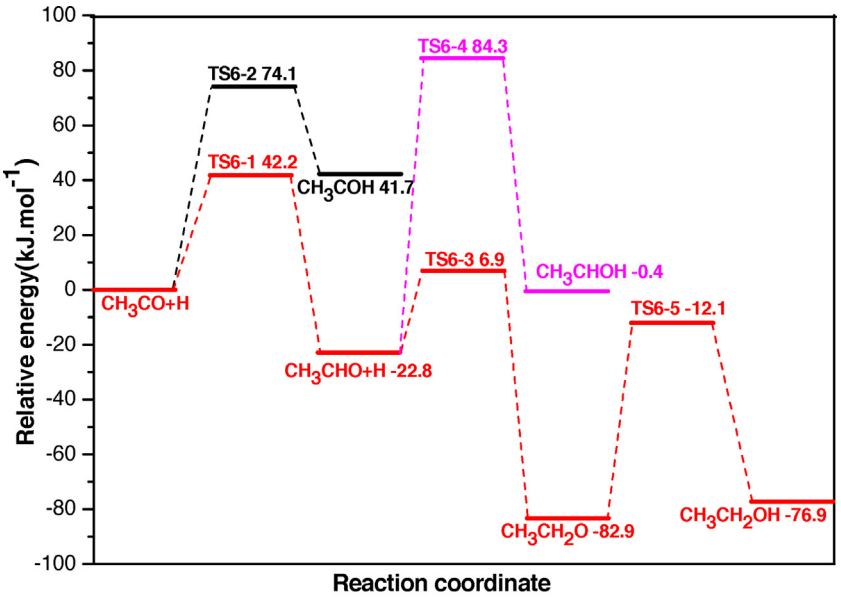

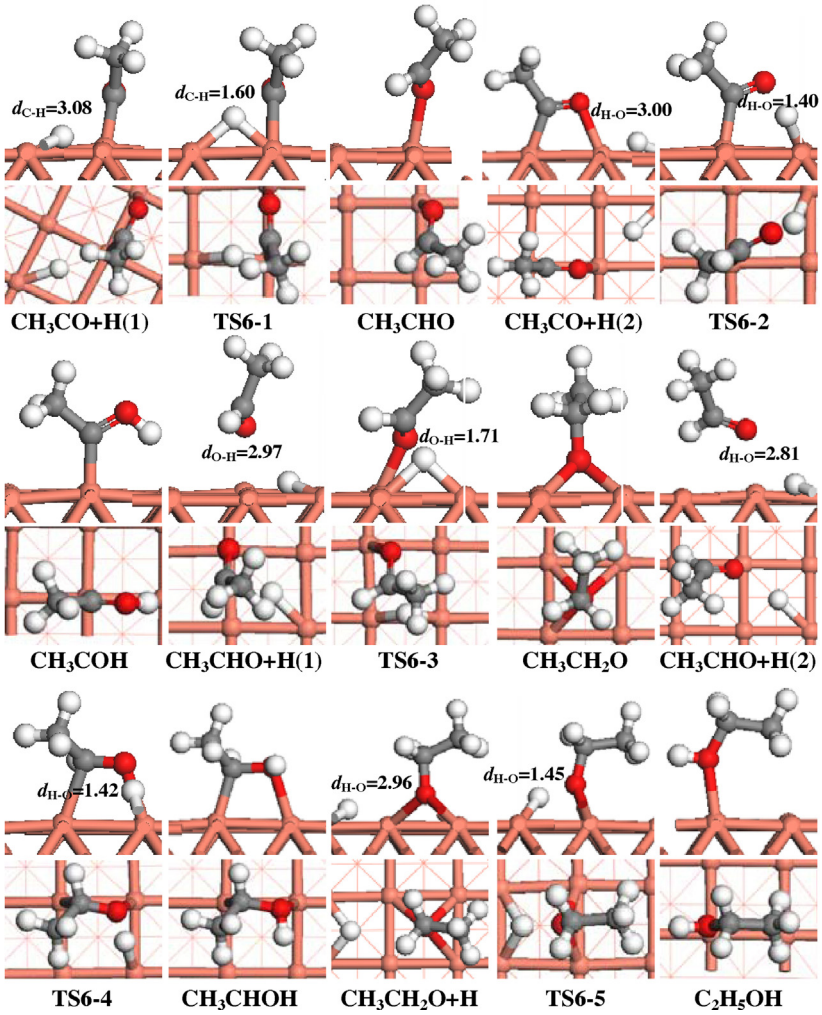

Fig. 13. The potential energy diagram of CH_3CO and CH_3CHO hydrogenation together with ISs, TSs and FSs on Cu(1 0 0) surface. Bond lengths are in Å. See Fig. 3 for color coding.

from syngas [29], and $CH_x(x=1–3)$ formation cannot compete with CH_3OH formation. Then, among all $CH_x(x=1–3)$ species, CH_3 are the most favorable species. Thus, the productivity and selectivity of C_2H_5OH is low due to less CH_3 sources on Cu(1 0 0) surface, and only two variables significantly affect the productivity and selectivity of C_2H_5OH, one is CH_3 formation, the other is CH_3OH formation. The productivity and selectivity of C_2H_5OH can be enhanced by lowering the activation barrier of

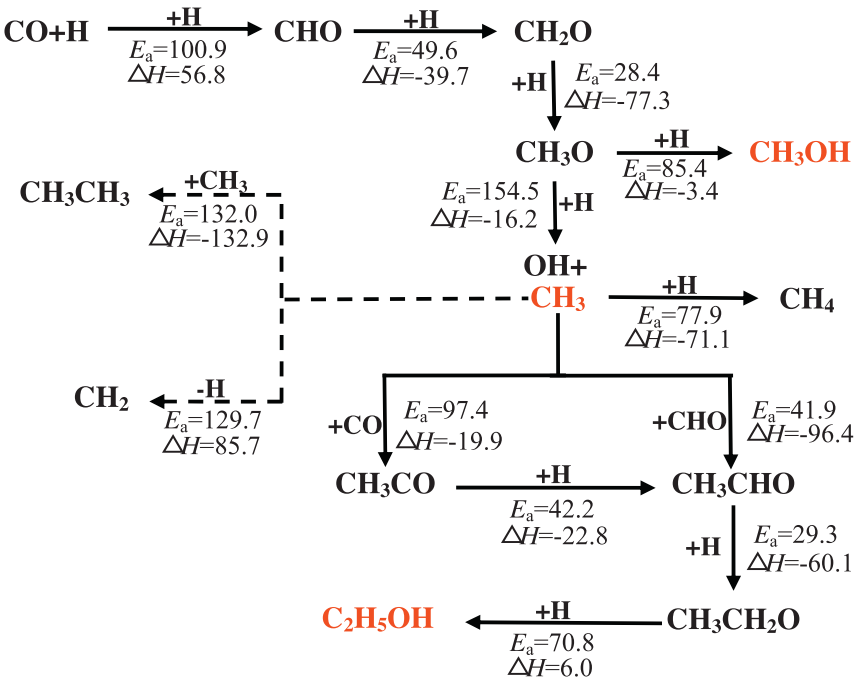

Fig. 14. Schematic of the optimal reaction pathway for C_2H_5OH synthesis from syngas on Cu(1 0 0) surface.

CH_3 formation and/or increase the activation barrier of CH_3OH formation.

On the basis of above results, we can obtain that when Cu-based catalysts are developed for C_2H_5OH formation from syngas, the catalytic performance of the materials toward the formations of CH_3 and CH_3OH have to be especially considered. To achieve high C_2H_5OH productivity and selectivity, promoters and/or supports used for Cu catalysts should maximizes CH_3 formation and/or minimizes CH_3OH formation, in this way, more CH_3 sources will be available for C_2 oxygenates formation of C_2H_5OH precursor by CHO insertion into CH_3, as a result, the productivity and selectivity of C_2H_5OH can be enhanced. On the other hand, the insight into reaction mechanism of C_2H_5OH formation from syngas on Cu catalyst not only obtain that how the Cu catalyst functions, but also predicts and provides a clue to selectively modify and develop the novel Cu-based catalyst to enhance the catalytic performance towards C_2H_5OH formation. In addition, extensive calculations for quantitative investigations into the effect of the promoters and/or supports on C_2H_5OH formation would be desirable, but this is beyond the scope of our present study, and will be carried out in our next work.

4. Conclusions

In the present study, the reaction mechanism of C_2H_5OH synthesis from syngas on Cu(1 0 0) surface has been systematically explored; here, our results are obtained using density functional theory method together with periodic slab model. The preference mechanism of C_2H_5OH formation from syngas has been obtained; two products, CH_3OH and C_2H_5OH, are mentioned in the overall conversion process. Our results show that ethanol formation from syngas starts with CHO formation by CO hydrogenation, in which the direct CO dissociation is difficult to occur. Starting from CHO, CHO is further hydrogenated to CH_3O via CH_2O intermediate, CH_3O eventually hydrogenates to form CH_3OH, and CH_3 is formed via CH_3O dissociation with hydrogen-assisted, in which CH_3OH is more easily formed than CH_3. Further, CHO insertion into CH_3 can form the key intermediate CH_3CHO, followed by the successive hydrogenation to C_2H_5OH via CH_3CH_2O intermediates, in which CHO insertion into CH_3 to CH_3CHO is the most favorable reaction among all reactions related to CH_3 species. In addition, Cu(1 0 0) surface is highly selective for CH_3OH rather than CH_3, further C_2H_5OH. Therefore, the productivity and selectivity of C_2H_5OH can be enhanced by lowering the activation barrier of CH_3 formation and/or increasing the activation barrier of CH_3OH formation, which means that promoters and/or supports should be added into Cu to help minimize CH_3OH formation and/or maximize CH_3 production.

Acknowledgment

This work is financially supported by the National Natural Science Foundation of China (No. 21276003, 21476155 and 21276171), the Natural Science Foundation of Shanxi Province (No. 2014011012-2), the Program for the Top Young Academic Leaders of Higher Learning Institutions of Shanxi, and the Top Young Innovative Talents of Shanxi.

Appendix A. Supplementary data

Supplementary data associated with this article can be found, in the online version, at http://dx.doi.org/10.1016/j.molcata.2015.04.015.

References

[1] R.G. Herman, Catal. Today 55 (2000) 233–245.
[2] V. Subramani, S.K. Gangwal, Energy Fuel 22 (2008) 814–839.
[3] J.J. Spivey, A. Egbebi, Chem. Soc. Rev. 36 (2007) 1514–1528.
[4] M. Gupta, M.L. Smith, J.J. Spivey, ACS Catal. 1 (2011) 641–656.
[5] J. Goldemberg, Science 315 (2007) 808–810.
[6] J.L. Gong, H.R. Yue, Y.J. Zhao, S. Zhao, L. Zhao, J. Lv, S.P. Wang, X.B. Ma, J. Am. Chem. Soc. 134 (2012) 13922–13925.
[7] Y.M. Choi, P. Liu, J. Am. Chem. Soc. 131 (2009) 13054–13061.
[8] N.D. Subramanian, G. Balaji, C.S.S.R. Kumar, J.J. Spivey, Catal. Today 147 (2009) 100–106.
[9] M.A. Haider, M.R. Gogate, R.J. Davis, J. Catal. 261 (2009) 9–16.
[10] P. Gronchi, E. Tempesti, C. Mazzocchia, Appl. Catal. A: Gen. 120 (1994) 115–126.
[11] Y.H. Zhao, M.M. Yang, D.P. Sun, H.Y. Su, K.J. Sun, X.F. Ma, X.H. Bao, W.X. Li, J. Phys. Chem. C 115 (2011) 18247–18256.
[12] L.P. Han, D.S. Mao, J. Yu, Q.S. Guo, G.Z. Lu, Catal. Commun. 23 (2012) 20–24.

[13] F.Y. Li, D.E. Jiang, X.C. Zeng, Z.F. Chen, Nanoscale 4 (2012) 1123–1129.
[14] N. Kapur, J. Hyun, B. Shan, J.B. Nicholas, K. Cho, J. Phys. Chem. C 114 (2010) 10171–10182.
[15] Y.H. Zhao, K.J. Sun, X.F. Ma, J.X. Liu, D.P. Sun, H.Y. Su, W.X. Li, Angew. Chem. Int. Ed. 50 (2011) 5335–5338.
[16] J.C. Slaa, J.G. van Ommen, J.R.H. Ross, Catal. Today 15 (1992) 129–148.
[17] R. Xu, W. Wei, W.H. Li, T.D. Hu, Y.H. Sun, J. Mol. Catal. A: Chem. 234 (2005) 75–83.
[18] R. Xu, C. Yang, W. Wei, W.H. Li, Y.H. Sun, T.D. Hu, J. Mol. Catal. A: Chem. 221 (2004) 51–58.
[19] N. Zhao, R. Xu, W. Wei, Y.H. Sun, React. Kinet. Catal. Lett. 75 (2002) 297–304.
[20] V. Mahdavi, M.H. Peyrovi, M. Islami, J.Y. Mehr, Appl. Catal. A: Gen. 281 (2005) 259–265.
[21] R.G. Zhang, B.J. Wang, H.Y. Liu, L.X. Ling, J. Phys. Chem. C 115 (2011) 19811–19818.
[22] D.H. Mei, M. Neurock, C.M. Smith, J. Catal. 268 (2009) 181–195.
[23] Z.P. Liu, P. Hu, J. Am. Chem. Soc. 125 (2003) 1958–1967.
[24] C.F. Huo, Y.W. Li, J.G. Wang, H.J. Jiao, J. Am. Chem. Soc. 131 (2009) 14713–14721.
[25] Y.H. Chin, C. Buda, M. Neurock, E. Iglesia, J. Catal. 283 (2011) 10–24.
[26] Y.X. Pan, C.J. Liu, Q.F. Ge, J. Catal. 272 (2010) 227–234.
[27] M. Behrens, F. Studt, I. Kasatkin, S. Kühl, M. Hävecker, F. Abild-Pedersen, S. Zander, F. Girgsdies, P. Kurr, B.-L. Kniep, M. Tovar, R.W. Fischer, J.K. Nørskov, R. Schlögl, Science 336 (2012) 893–897.
[28] X.C. Sun, R.G. Zhang, B.J. Wang, Appl. Surf. Sci. 265 (2013) 720–730.
[29] R.G. Zhang, X.C. Sun, B.J. Wang, J. Phys. Chem. C 117 (2013) 6594–6606.
[30] R.G. Zhang, G.R. Wang, B.J. Wang, J. Catal. 305 (2013) 238–255.
[31] L.C. Grabow, M. Mavrikakis, ACS Catal. 1 (2011) 365–384.
[32] G.C. Wang, J. Nakamura, J. Phys. Chem. Lett. 1 (2010) 3053–3057.
[33] G.C. Wang, L. Jiang, Z.S. Cai, Y.M. Pan, X.Z. Zhao, W. Huang, K.C. Xie, Y.W. Li, Y.H. Sun, B. Zhong, J. Phys. Chem. B 107 (2003) 557–562.
[34] X.Y. Pang, C. Wang, Y.H. Zhou, J.M. Zhao, G.C. Wang, J. Mol. Struct.: Theochem 948 (2010) 1–10.
[35] M.Ø. Pedersen, L. Österlund, J.J. Mortensen, M. Mavrikakis, L.B. Hansen, I. Stensgaard, E. Lægsgaard, J.K. Nørskov, F. Besenbacher, Phys. Rev. Lett. 84 (2000) 4898–4901.
[36] G. Kresse, J. Furthmüller, Phys. Rev. B 54 (1996) 11169–11186.
[37] G. Kresse, J. Furthmüller, Comp. Mater. Sci. 6 (1996) 15–50.
[38] G. Kresse, D. Joubert, Phys. Rev. B 59 (1999) 1758–1775.
[39] J.P. Perdew, K. Burke, M. Ernzerhof, Phys. Rev. Lett. 77 (1996) 3865–3868.
[40] J.P. Perdew, J.A. Chevary, S.H. Vosko, K.A. Jackson, M.R. Pederson, D.J. Singh, C. Fiolhais, Phys. Rev. B 46 (1992) 6671–6687.
[41] H.J. Monkhorst, J.D. Pack, Phys. Rev. B 13 (1976) 5188–5192.
[42] M. Methfessel, A.T. Paxton, Phys. Rev. B 40 (1989) 3616–3621.
[43] D. Sheppard, P. Xiao, W. Chemelewski, D.D. Johnson, G. Henkelman, J. Chem. Phys. 136 (2012) 074103-01–074103-08.
[44] D. Sheppard, R. Terrell, G. Henkelman, J. Chem. Phys 128 (2008) 134106-01–134106-10.
[45] G. Henkelman, H. Jónsson, J. Chem. Phys. 111 (1999) 7010–7022.
[46] R.A. Olsen, G.J. Kroes, G. Henkelman, A. Arnaldsson, H. Jónsson, J. Chem. Phys. 121 (2004) 9776–9792.
[47] R.G. Zhang, L.X. Ling, B.J. Wang, W. Huang, Appl. Surf. Sci. 256 (2010) 6717–6722.
[48] B.Z. Sun, W.K. Chen, J.D. Zheng, C.H. Lu, Appl. Surf. Sci. 255 (2008) 3141–3148.
[49] N. Jardillier, E.A. Villagomez, G. Delahay, B. Coq, D. Berthomieu, J. Phys. Chem. B 110 (2006) 16413–16421.
[50] D. Loffreda, P. Sautet, J. Phys. Chem. B 109 (2005) 9596–9603.
[51] C. Weilach, S.M. Kozlov, H.H. Holzapfel, K. Föttinger, K.M. Neyman, G. Rupprechter, J. Phys. Chem. C 116 (2012) 18768–18778.
[52] C. Yang, Z.Y. Ma, N. Zhao, W. Wei, T.D. Hu, Y.H. Sun, Catal. Today 115 (2006) 222–227.
[53] Y.X. Yang, M.G. White, P. Liu, J. Phys. Chem. C 116 (2011) 248–256.
[54] H.J. Li, C.C. Chang, J.J. Ho, J. Phys. Chem. C 115 (2011) 11045–11055.
[55] Q.F. Zhang, B. Han, X.W. Tang, K. Heier, J.X. Li, J. Hoffman, M.F. Lin, S.L. Britton, A. Derecskei-Kovacs, H.S. Cheng, J. Phys. Chem. C 116 (2012) 16522–16531.
[56] M. Ojeda, A. Li, R. Nabar, A.U. Nilekar, M. Mavrikakis, E. Iglesia, J. Phys. Chem. C 114 (2010) 19761–19770.
[57] I.N. Remediakis, F. Abild-Pedersen, J.K. Nørskov, J. Phys. Chem. B 108 (2004) 14535–14540.
[58] X.K. Gu, W.X. Li, J. Phys. Chem. C 114 (2010) 21539–21547.
[59] S. Lin, R.S. Johnson, G.K. Smith, D.Q. Xie, H. Guo, Phys. Chem. Chem. Phys. 13 (2011) 9622–9631.
[60] S. Lin, D.Q. Xie, H. Guo, J. Phys. Chem. C 115 (2011) 20583–20589.
[61] S.C. Chuang, R.J. Stevens, R. Khatri, Top. Catal. 32 (2005) 225–232.